On the high-temperature degradation mechanism of ZnO-based thermoelectrics

Blanca I. Arias-Serrano [1*], Sergey M. Mikhalev [2], Marta C. Ferro [1], David M. Tobaldi [1], Jorge R. Frade [1], Andrei V. Kovalevsky [1]*

[1] CICECO – Aveiro Institute of Materials, Department of Materials and Ceramic Engineering, University of Aveiro, 3810-193 Aveiro, Portugal;
[2] TEMA-NRD, Mechanical Engineering Department, Aveiro Institute of Nanotechnology (AIN), University of Aveiro, 3810-193 Aveiro, Portugal

* Corresponding authors. Present address: Department of Materials and Ceramic Engineering, CICECO, University of Aveiro, 3810-193 Aveiro, Portugal.
e-mails: blanca@ua.pt; akavaleuski@ua.pt

Abstract

The stability and reproducibility of the electric properties in n-type doped ZnO represent known bottlenecks towards potential thermoelectric applications. The degradation is promoted by the vanishing of the electronic defects on oxidation and irreversible exsolution of the phase impurities. This work proposes a microstructural mechanism showing that these processes take place mainly in the pores and highlighting the necessity for high densification of ZnO-based thermoelectrics to ensure more stable operation. The electrical performance was monitored at various temperatures, followed by a detailed microstructural analysis. The evolution of the electrical conductivity and Seebeck coefficient confirm that the degradation is related to a gradual decrease in the charge carrier concentration rather than to the effects suppressing their mobility. The results suggest that the donor exsolution may promote an increase or decrease of the power factor, guided by the self-optimization of the charge carrier concentration.

Keywords: zinc oxide; thermoelectrics; degradation mechanism; microstructural evolution; electrical properties

1. Introduction

Zinc oxide represents a versatile platform for a range of multifunctional materials with promising electrical, catalytic, photochemical and optoelectronic properties [1,2]. The discovery of relative high charge carrier mobility in aluminium-doped zinc oxide, stemming from covalent bonding and a small difference in electronegativity between zinc and oxygen [3], have boosted the research focusing on thermoelectric applications of this material. Among other oxides, n-doped ZnO features an excellent electrical performance, combined, however, with a relatively high thermal conductivity [4-8]. Doping relies on transition metal cations and aluminium, possessing the oxidation state higher than 2+ and fitting the size and coordination preferences of the wurtzite structure [3,9,10-13]. A promising direction towards minimizing the thermal conductivity is represented by the engineering of the nano-grained ceramics and nanocomposite concepts [4,14,15].

Another bottleneck limiting the potential application of ZnO-based thermoelectrics is the deterioration of the electrical performance with time on heating in ambient air [4,7,12,16,17]. In this way, the major advantage of thermal stability, inherent to oxide thermoelectrics as compared to traditional Bi_2Te_3, Bi_2Se_3, PbTe materials, is compromised for ZnO. The degradation in oxygen-rich atmospheres is usually attributed to the oxygen uptake, reducing the mobility of the charge carriers at the grain boundaries, and formation of the phase impurities [7,8,12,16,17]. Although general reasons for this behaviour are mostly clear, no microstructural guidelines for the degradation mechanism are yet proposed. The degradation is mostly discussed in terms of the variations in electrical conductivity, without taking into account combined effects on the power factor. Our work takes this opportunity by considering the time evolution of the electrical conductivity and Seebeck coefficient at relevant temperatures, analyzed in combination with post-mortem microstructural studies. Three typical dopants promoting n-type semiconducting behaviour in ZnO were selected,

including aluminium, iron and zirconium [3,9-11,18]. There is significant scattering in the solubility limits of donor-doped ZnO materials which is often linked to diverse conditions employed for synthesis and subsequent thermal treatments. Available literature date on the solubility of aluminum and iron in ZnO varies from 1 [19] to 0.3-0.25 at.% [3,20] and from 1.5 [21] to 0.7-0.5 at.% [22], respectively. In the case of zirconium, solubility has been reported to be less than 0.04 at.% [23]. The general composition $Zn_{0.996}Me_{0.004}O$ ensures the same doping level, which is moderate enough to minimize the phase impurities and blocking effects at the grain boundaries while being sufficient to impart a reasonable thermoelectric performance.

2. Experimental procedure

The set of ceramic samples with a nominal composition $Zn_{0.996}Me_{0.004}O$ (Me – Fe, Al, Zr) and pristine ZnO was processed by conventional solid-state route using simple oxide precursors. The stoichiometric amounts of precursor´s powders were dispersed in alcohol to form a suspension, which was gradually dried while mixed by ultrasound. The resulting dry mixtures were compacted using a preliminary uniaxial pressing followed by the final cold isostatic pressing step at 200 MPa. Thus obtained green disc-shaped samples were sintered at 1773 K for 10 h in air to produce ceramics. According to previous works [4,9,13], this temperature will produce dense ceramics while maintaining possible Zn volatilization at a moderate enough level to minimize phase impurities and blocking effects at the grain boundary. The doping level of the as-sintered ceramics is therefore expected to be slightly higher compare to the nominal, although the choice of the dopant is not expected to impact Zn losses so that the chemical composition remains comparable. In order to obtain less dense $Zn_{0.996}Fe_{0.004}O$ ceramics, the dried precursor's mixture was annealed at 1223 K for 6 hours

before the compacting step to coarsen the powder. Further on, the freshly-sintered samples are referred to as "as-prepared".

XRD studies were performed for the powdered samples, obtained by grinding of sintered ceramics. Scanning electron microscopy coupled with energy dispersive spectroscopy (SEM/EDS) was involved for microstructural characterization of both polished samples after thermal etching and fractured ceramics. Electrical conductivity and Seebeck coefficient were measured on bar-shaped samples with the typical dimensions of ~1.5×2.5×15 mm^3.

Room-temperature XRD patterns were recorded on PANalytical X'Pert PRO diffractometer (CuKα), with a step of 0.02° in the range 2Θ=10°–80° using an exposition time of 200 s. For the microstructural studies, Hitachi SU-70 instrument (SEM) equipped with a Bruker Quantax 400 detector (EDS) was used. The experimental setup for well-controlled simultaneous measurements of the electrical conductivity (σ) and Seebeck coefficient (α) is described elsewhere (see Ref. [24] and references cited). The studies were done at 450-1173 K in flowing air. Two measurement procedures were implemented. First one simulated a typical route involved in thermoelectric characterization, assuming that, after thermal equilibration, no offset effects on the transport properties are present. This included stepwise cooling from 1173 K with dwells of 15-30 min, followed by recording the electrical properties and the next step. As a rule, the reproducibility error did not exceed 5–9% [4]. The uncertainty of temperature gradient measurement at 1173 K was below 4% for the applied gradients ΔT of 15-20 K. The second mode to access the degradation relied on the isothermal measurements in flowing air after fast heating of the as-prepared samples to 973 K, followed by 1173 K. At each of these temperatures, the electrical conductivity and Seebeck coefficient were continuously monitored during 25-30 h.

3. Results and discussion

Typical XRD patterns of the as-prepared samples shown in Fig. 1A and Fig. S1 suggest apparently single-phase composition for all as-prepared samples.

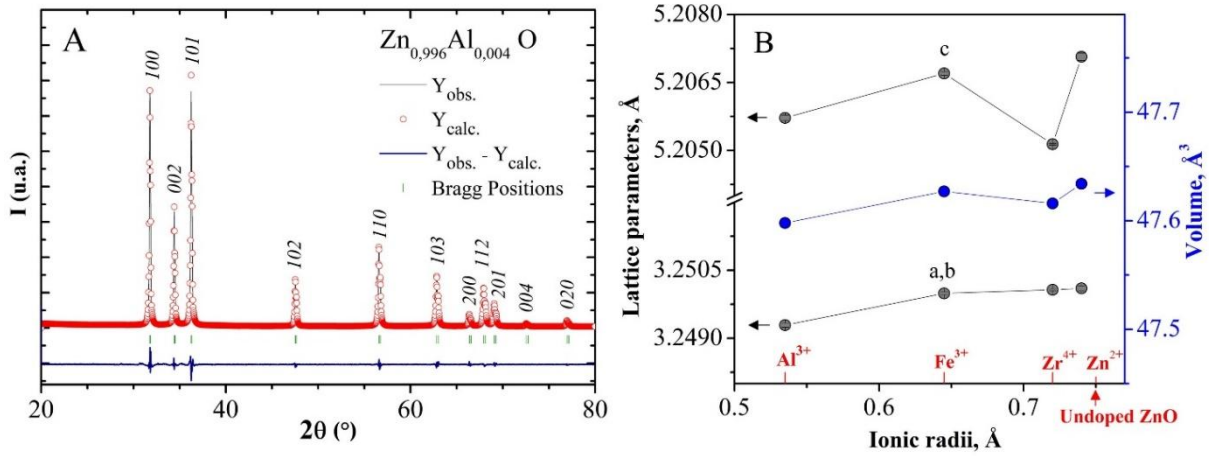

Fig. 1. XRD pattern of as-prepared $Zn_{0.996}Al_{0.004}O$ sample (A) and composition dependence of the lattice parameters and unit cell volume described in terms of the ionic radii [25].

All reflections belong to a hexagonal wurtzite structure, indexed following ICDD reference pattern 04-009-7657. Differences in the relative intensity of the three main peaks (1 0 0) (2 0 0) and (1 0 1) at 2θ equal to 31.76, 34.43 and 36.26°, respectively, were noticeable for $Zn_{0.996}Al_{0.004}O$ and for $Zn_{0.996}Fe_{0.004}O$ with respect to the reference pattern. This phenomenon has been related to the presence of crystallographic preferred orientations [26-29]. However, owing to the relatively weak texture of all prepared samples, we do not anticipate an anisotropic response regarding overall thermoelectric and transport properties. No signs of the monoclinic ZrO_2 phase were observed for $Zn_{0.996}Zr_{0.004}O$, while chemical mapping reveals corresponding inclusions (Fig. S2). This situation is typical for doped ZnO-based materials [4]. The ZnO wurtzite structure is capable of accommodating only a limited amount of the transition metal cation, except for Mn and Co [1,9]. Nominally low dopant content complicates establishing the solubility limit and identification of the doping excess, which is often below the detection limit of a typical XRD equipment. The solubility is mainly

determined by the cationic size and charge mismatch, while its low level only slightly affects the lattice parameters and the unit cell volume (Fig. 1B). Similarly to Ta^{5+} [13], a high charge difference between host and dopant cations may lead to the formation of the dislocations, with a substantial impact on the *c* parameter [1] as in the case of Zr^{4+} (Fig. 1B). In general, these results mostly confirm the suitability of the selected samples for further studies.

The electrical properties of the as-prepared samples, measured on stepwise cooling, are shown in Fig. 2.

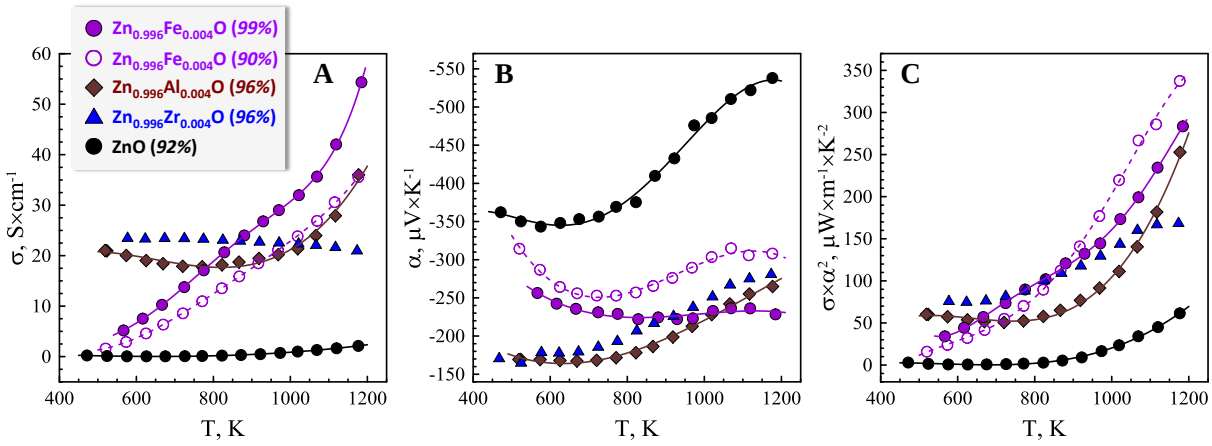

Fig. 2. Temperature dependence of the electrical conductivity (A), Seebeck coefficient (B) and power factor (C), measured in the conditions of relatively fast thermal equilibration of the sample at each temperature.

As expected, all doped samples demonstrate a higher electrical performance compared to pristine ZnO, which represents a natural n-type semiconductor with intrinsic defects, including oxygen vacancies and zinc interstitials [1]. The obtained values for electrical properties are within the typical ranges reported in the literature [3,9-11,18]; the transition from thermally-activated semiconducting to metallic behaviour is also often observed and discussed in terms of the changes in charge carrier concentration and scattering mechanisms [12]. The charge carriers are generated by the following reaction, exemplifying the case of doping with iron:

$$\frac{x}{2}Fe_2O_3 + (1-x)ZnO \rightarrow xFe_{Zn}^{\bullet} + xe^- + (1-x)Zn_{Zn}^{x} + O_O^x + \frac{x}{4}O_2(g) \qquad \text{(Eq. 1)}$$

In pristine ZnO, which is known as a native n-type semiconductor, intrinsic defects including Zn interstitials and oxygen vacancies are formed by Frenkel and Schottky reactions, correspondingly, and generate electrons [30]:

$$Zn_i^X \leftrightarrow Zn_i^{\bullet\bullet} + 2e^- \qquad \text{(Eq. 2)}$$

$$V_O^X \leftrightarrow V_O^{\bullet\bullet} + 2e^- \qquad \text{(Eq. 3)}$$

These reactions are reversible and may instead trap the charge carriers, leading to lower electrical conductivity and higher Seebeck coefficient. The pair defects, which accompany the formation of Zn interstitials and oxygen vacancies, include zinc vacancies and oxygen interstitials. These defects may localize at the grain boundaries, creating acceptor states and potential barriers, impeding the transport of the charge carriers [7]. Thus, the defect chemistry of zinc oxide is inherently complex and results in significant variations of the electrical properties (Fig. 2A,B) with composition and temperature even for the same dopant content. The impacts imposed by a moderate difference in the porosity of the $Zn_{0.996}Fe_{0.004}O$ sample also cannot be predicted by using a simple mixing rule. It should be noticed that all studied samples possess the density above 90% of theoretical, in good agreement with the microstructural studies (Fig. S3). Finally, a significant variation of the power factor for a similar dopant content is also observed (Fig. 2C).

A discrepancy in the reported thermoelectric performances for donor-doped ZnO is often linked to the deterioration over time, with a strong dependence on the thermal prehistory [4,12,16]. The electrical performance is usually monitored as a function of temperature for the samples after different thermal cycles and/or redox treatments [7,8,12,16,17]. A somewhat different approach to evaluate the relevant degradation mechanisms is used in the present work, where the electrical properties were monitored overtime at two temperatures (Fig. 3).

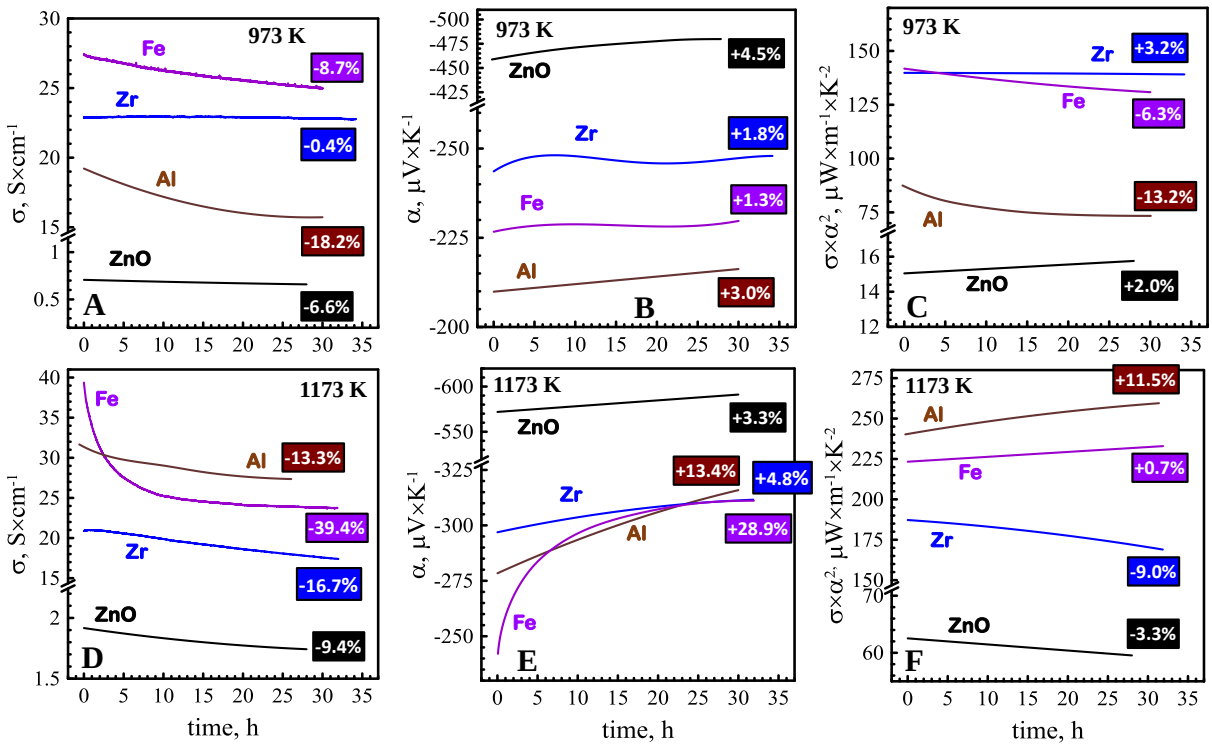

Fig. 3. Time dependence of the electrical conductivity (A, D), Seebeck coefficient (B, E) and power factor (C, F) at 973 K (A–C) and 1173 K (D-F). The extent of evolution for each property is shown in % for each composition.

Noticeable changes in electrical conductivity and Seebeck coefficient are already observed at 973 K. The conductivity decrease is accompanied by a concomitant increase in Seebeck coefficient, suggesting a gradual vanishing of the charge carriers as a possible degradation mechanism, in opposite to possible suppressing of their mobility. The changes are more pronounced for $Zn_{0.996}Fe_{0.004}O$. Higher temperature (1173 K) promotes even faster degradation, as expected for thermal activation.

An insight into the microstructural mechanism of this degradation can be obtained from SEM/EDS studies of the samples before and after isothermal electrical measurements. Fig. 4 shows corresponding micrographs and elemental maps for $Zn_{0.996}Fe_{0.004}O$, a composition showing more pronounced changes in the electrical performance.

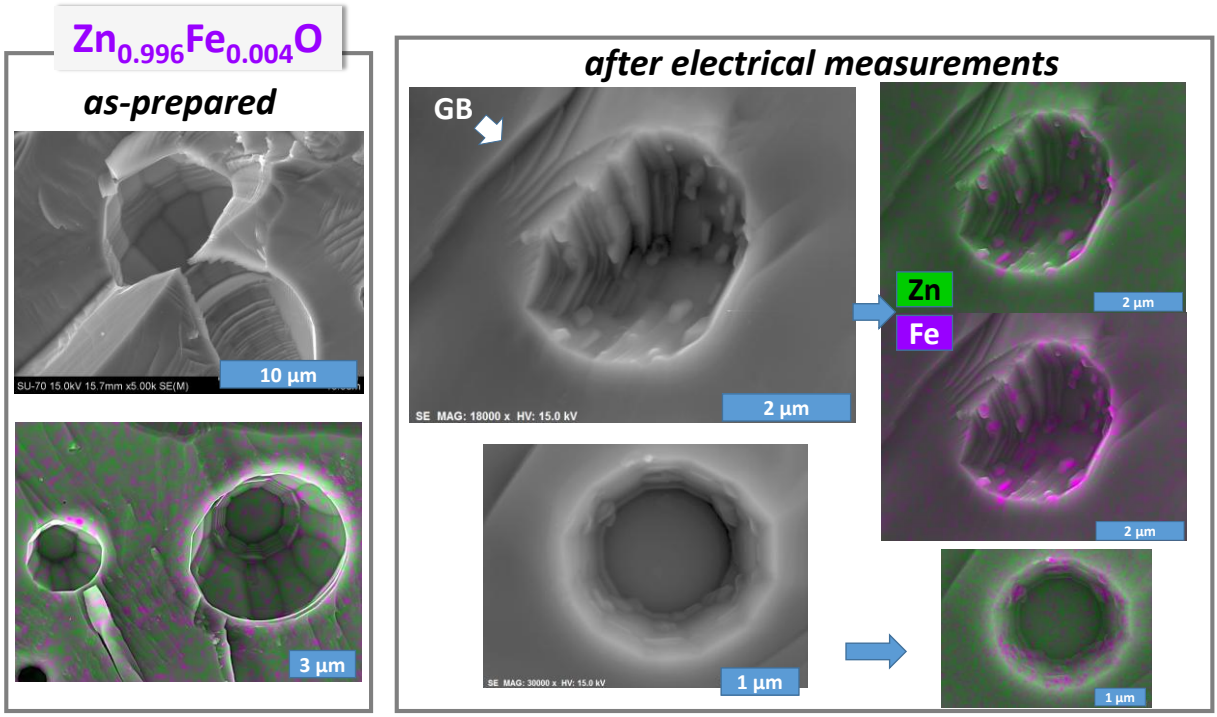

Fig. 4. SEM images and EDS chemical mapping results for the fractured $Zn_{0.996}Fe_{0.004}O$ samples, as-prepared and after electrical characterization.

The samples before electrical measurement are chemically homogeneous except for $Zn_{0.996}Zr_{0.004}O$, in good agreement with the XRD data (Fig. S1). However, while the XRD studies did not reveal any evolution in the phase composition after electrical measurements, the combined SEM/EDS analysis shows noticeable changes, taking place mainly in the pores. Iron-rich nanostructures grown at the pore walls likely correspond to $ZnFe_2O_4$ spinel [11], which is further not observed neither in ceramics bulk nor at the grain boundaries; this may be related to the strong temperature dependence of solubility of iron oxide at high temperatures [31], and uncertainties concerning the $ZnO/ZnFe_2O_4$ boundary at intermediate temperatures. Relatively fast cooling of the ceramics after sintering at high temperature mostly avoids the impurity segregation and freezes the high-temperature defect structure [16]. During following high-temperature measurements, the oxygen exchange is facilitated in the pores, where less geometrical restrictions to the formation of the new phase also exist. The phase exsolution is

also expected to be confined in the dense ceramic bulk. Thus, the microstructural mechanism of the high-temperature degradation likely involves the irreversible exsolution of the dopant-containing species predominantly in the pores, consuming the charge carriers:

$$2Fe_{Zn}^{\bullet} + Zn_{Zn}^{x} + 3O_{O}^{x} + 2e^{-} + 0.5O_2 \rightarrow ZnFe_2O_4 \qquad \text{(Eq. 4)}$$

In the case of doping with aluminium, the precipitation of $ZnAl_2O_4$ spinel phase is also mainly observed in the pores, as compared to the as-prepared sample (Fig. S4). Thus, even a slight excess of porosity in mostly dense ceramic samples may result in corresponding variations of the electrical performance, as illustrated for $Zn_{0.996}Fe_{0.004}O$ (Fig. 2), unambiguously suggesting a decrease of the charge carrier concentration. The pristine ZnO also demonstrates a noticeable degradation (Fig. 3), which, in this case, can be promoted by oxidation and filling the oxygen vacancies at the open surfaces. Unfortunately, the initial presence of the phase impurities in $Zn_{0.996}Zr_{0.004}O$ does not allow to follow the microstructural aspects of the degradation in this composition (Fig. S2). Though, the dynamic behaviour of its electrical properties is essentially similar to other compositions.

In general, these observations imply that very high densification is crucial to minimize high-temperature degradation. Porosity effects should be further studied, taking into account that frozen defect structure of as-prepared samples with modulated porosity may depend on the cooling conditions. Fast quenching of the samples after sintering may be involved. Nevertheless, the obtained results unambiguously demonstrate that even residual porosity may notably affect electrical performance. At the same time, the exsolution of spinel phases at nanoscale usually is favourable for suppressing the thermal conductivity in ZnO-based materials [15,32], although possible compromise between phonon scattering ability of the point defects (e.g., $Fe_{Zn}^{\bullet}$, $Al_{Zn}^{\bullet}$ and $Zr_{Zn}^{\bullet\bullet}$) in the crystal structure and nanointerfaces induced by the exsoluted phases should be also taken into account [33]. A simple assessment of the power factor during degradation (Fig. 3 C,F) suggests that this process, while effectively

resulting in donor exsolution, may actually even improve the thermoelectric performance in some cases. Although it seems counterintuitive from the first look, the underlying reason is likely linked to a self-optimization of the charge carrier concentration, compromising the trade-off between electrical conductivity and Seebeck coefficient [34]. However, this behaviour is somewhat difficult to account for in real thermoelectric modules, where stable performance is one of the main requirements.

4. Conclusions

In this work, a set of ceramic materials with a nominal composition $Zn_{0.996}Me_{0.004}O$ (Me – Fe, Al, Zr) was prepared by the conventional solid-state route and exploited for the studies of the degradation of thermoelectric performance. XRD analysis combined with SEM/EDS microstructural characterization confirmed the formation of single-phase wurtzite, except for $Zn_{0.996}Zr_{0.004}O$ composition. Continuous monitoring of the electrical properties at 973 K and 1173 K revealed the presence of transient processes, resulting in up to ~40% electrical conductivity drop and ~30% enhancement in Seebeck coefficient during first 30-35 h for $Zn_{0.996}Fe_{0.004}O$ at 1173 K. Similar tendencies were observed for other prepared materials, including pristine ZnO. Comparative analysis of the microstructural evolution of the samples during degradation have suggested a possible mechanism related to the exsolution of $ZnAl_2O_4$ and $ZnFe_2O_4$ spinels, which takes place predominantly in the pores, even in the case of residual porosity. The obtained results demonstrated that these processes not necessarily lead to the deterioration of the overall electrical performance, described by the power factor.

Acknowledgements

This work was supported by the project CICECO-Aveiro Institute of Materials (ref. UIDB/50011/2020 & UIDP/50011/2020) and the project POCI-01-0145-FEDER-031875, financed by COMPETE 2020 Program and National Funds through the FCT/MEC and when applicable co-financed by FEDER under the PT2020 Partnership Agreement. Sergey M. Mikhalev and David M. Tobaldi acknowledge the support of national funds (OE), through FCT – Fundação para a Ciência e a Tecnologia, I.P., in the scope of the framework contract foreseen in the numbers 4, 5 and 6 of the article 23, of the Decree-Law 57/2016, of August 29, changed by Law 57/2017, of July 19.

References

[1] H. Morkoç, Ü. Özgür, Zinc Oxide: Fundamentals, Materials and Device Technology, Wiley-VCH Verlag GmbH & Co. KGaA, Weinheim, Germany, Germany, 2009. https://doi.org/10.1002/9783527623945.

[2] C.F. Klingshirn, ZnO: Material, physics and applications, ChemPhysChem. 8 (2007) 782–803. https://doi.org/10.1002/cphc.200700002.

[3] T. Tsubota, M. Ohtaki, K. Eguchi, H. Arai, Thermoelectric properties of Al-doped ZnO as a promising oxide material for high-temperature thermoelectric conversion, J. Mater. Chem. 7 (1997) 85–90. https://doi.org/10.1039/a602506d.

[4] K.V. Zakharchuk, M. Widenmeyer, D.O. Alikin, W. Xie, S. Populoh, S.M. Mikhalev, A. Tselev, J.R. Frade, A. Weidenkaff, A.V. Kovalevsky, A self-forming nanocomposite concept for ZnO-based thermoelectrics, J. Mater. Chem. A. 6 (2018) 13386–13396. https://doi.org/10.1039/c8ta01463a.

[5] D.-B. Zhang, H.-Z. Li, B.-P. Zhang, D. Liang, M. Xia, Hybrid-structured ZnO thermoelectric materials with high carrier mobility and reduced thermal conductivity, RSC Adv. 7 (2017) 10855–10864. https://doi.org/10.1039/C6RA28854E.

[6] P. Jood, R.J. Mehta, Y. Zhang, T. Borca-Tasciuc, S.X. Dou, D.J. Singh, G. Ramanath, Heavy element doping for enhancing thermoelectric properties of nanostructured zinc oxide, RSC Adv. 4 (2014) 6363. https://doi.org/10.1039/c3ra46813e.

[7] T. Tian, L. Cheng, L. Zheng, J. Xing, H. Gu, S. Bernik, H. Zeng, W. Ruan, K. Zhao, G. Li, Defect engineering for a markedly increased electrical conductivity and power factor in doped ZnO ceramic, Acta Mater. 119 (2016) 136–144. https://doi.org/10.1016/j.actamat.2016.08.026.

[8] F. Giovannelli, C. Chen, P. Díaz-Chao, E. Guilmeau, F. Delorme, Thermal conductivity and stability of Al-doped ZnO nanostructured ceramics, J. Eur. Ceram. Soc. 38 (2018) 5015–5020. https://doi.org/10.1016/j.jeurceramsoc.2018.07.032.

[9] K. V. Zakharchuk, D.M. Tobaldi, X. Xiao, W. Xie, S.M. Mikhalev, J.F. Martins, J.R. Frade, A. Weidenkaff, A. V. Kovalevsky, Synergistic effects of zirconium- and aluminum co-doping on the thermoelectric performance of zinc oxide, J. Eur. Ceram. Soc. 39 (2019) 1222–1229. https://doi.org/10.1016/j.jeurceramsoc.2018.11.029.

[10] E. Guilmeau, A. Maignan, C. Martin, Thermoelectric oxides: Effect of doping in delafossites and zinc oxide, J. Electron. Mater. 38 (2009) 1104–1108. https://doi.org/10.1007/s11664-009-0815-2.

[11] X. Liang, Thermoelectric transport properties of Fe-enriched ZNO with high-temperature nanostructure refinement, ACS Appl. Mater. Interfaces. 7 (2015) 7927–7937. https://doi.org/10.1021/am509050a.

[12] L. Han, D. V. Christensen, A. Bhowmik, S.B. Simonsen, L.T. Hung, E. Abdellahi, Y.Z. Chen, N. V. Nong, S. Linderoth, N. Pryds, Scandium-doped zinc cadmium oxide as a new stable n-type oxide thermoelectric material, J. Mater. Chem. A. 4 (2016) 12221–12231. https://doi.org/10.1039/C6TA03126A.

[13] B.I. Arias-Serrano, W. Xie, M.H. Aguirre, D.M. Tobaldi, A.R. Sarabando, S. Rasekh, S.M. Mikhalev, J.R. Frade, A. Weidenkaff, A. V. Kovalevsky, Exploring Tantalum as a Potential Dopant to Promote the Thermoelectric Performance of Zinc Oxide, Materials (Basel). 12 (2019) 2057. https://doi.org/10.3390/ma12132057.

[14] L. Han, N. Van Nong, W. Zhang, L.T. Hung, T. Holgate, K. Tashiro, M. Ohtaki, N. Pryds, S. Linderoth, Effects of morphology on the thermoelectric properties of Al-doped ZnO, R. Soc. Chem. Adv. 4 (2014) 12353. https://doi.org/10.1039/c3ra47617k.

[15] P. Jood, R.J. Mehta, Y. Zhang, G. Peleckis, X. Wang, R.W. Siegel, T. Borca-Tasciuc, S.X. Dou, G. Ramanath, Al-doped zinc oxide nanocomposites with enhanced thermoelectric properties, Nano Lett. 11 (2011) 4337–4342. https://doi.org/10.1021/nl202439h.

[16] N. Vogel-Schäuble, R. Dujardin, A. Weidenkaff, M.H. Aguirre, Influence of thermal aging phenomena on thermoelectric properties of al-substituted ZnO, J. Electron. Mater. 41 (2012) 1606–1614. https://doi.org/10.1007/s11664-011-1851-2.

[17] T. Minami, T. Miyata, T. Yamamoto, Stability of transparent conducting oxide films for use at high temperatures, J. Vac. Sci. Technol. a-Vacuum Surfaces Film. 17 (1999) 1822–1826. https://doi.org/10.1116/1.581897.

[18] D. Bérardan, C. Byl, N. Dragoe, Influence of the preparation conditions on the thermoelectric properties of Al-doped ZnO, J. Am. Ceram. Soc. 93 (2010) 2352–2358. https://doi.org/10.1111/j.1551-2916.2010.03751.x.

[19] K.H. Kim, S.H. Shim, K.B. Shim, K. Niihara, J. Hojo, Microstructural and thermoelectric characteristics of zinc oxide- based thermoelectric materials fabricated using a spark plasma sintering process, J. Am. Ceram. Soc. 88 (2005) 628–632.

[20] K. Shirouzu, T. Ohkusa, M. Hotta, N. Enomoto, J. Hojo, Distribution and solubility limit of Al in Al2O3-doped ZnO sintered body, J. Ceram. Soc. Japan. 115 (2007) 254–258.

[21] S.G. Protasova, B.B. Straumal, A.A. Mazilkin, S. V Stakhanova, P.B. Straumal, B. Baretzky, Increase of Fe solubility in ZnO induced by the grain boundary adsorption, J. Mater. Sci. 49 (2014) 4490–4498.

[22] B. Alemán, Y. Ortega, J.Á. García, P. Fernández, J. Piqueras, Fe solubility, growth mechanism, and luminescence of Fe doped ZnO nanowires and nanorods grown by evaporation-deposition, J. Appl. Phys. 110 (2011) 14317.

[23] G. Murtaza, R. Ahmad, M.S. Rashid, M. Hassan, A. Hussnain, M.A. Khan, M.E. ul Haq, M.A. Shafique, S. Riaz, Structural and magnetic studies on Zr doped ZnO diluted magnetic semiconductor, Curr. Appl. Phys. 14 (2014) 176–181.

[24] A.V. V. Kovalevsky, A.A.A. Yaremchenko, S. Populoh, A. Weidenkaff, J.R.R. Frade, Enhancement of thermoelectric performance in strontium titanate by praseodymium substitution, J. Appl. Phys. 113 (2013) 053704. https://doi.org/10.1063/1.4790307.

[25] R.D. Shannon, Revised Effective Ionic Radii and Systematic Studies of Interatomie Distances in Halides and Chaleogenides Central Research and Development Department , Experimental Station , E . L Du Pont de Nemours The effective ionic radii of Shannon & Prewitt [Acta, Acta Cryst. A32 (1976) 751–767. https://doi.org/10.1107/S0567739476001551.

[26] P. Díaz-Chao, F. Giovannelli, O. Lebedev, D. Chateigner, L. Lutterotti, F. Delorme, E. Guilmeau, Textured Al-doped ZnO ceramics with isotropic grains, J. Eur. Ceram. Soc. 34 (2014) 4247–4256.

[27] J.L. Ning, K.H. Kim, K.B. Shim, Influence of texture on electrical properties of ZnO ceramics prepared by extrusion and spark plasma sintering, Ceram. Int. 33 (2007) 107–114.

[28] H. Kaga, Y. Kinemuchi, S. Tanaka, A. Makiya, Z. Kato, K. Uematsu, K. Watari, Preparation and thermoelectric property of highly oriented Al-doped ZnO ceramics by a high magnetic field, Jpn. J. Appl. Phys. 45 (2006) L1212.

[29] M. Søndergaard, E.D. Bøjesen, K.A. Borup, S. Christensen, M. Christensen, B.B. Iversen, Sintering and annealing effects on ZnO microstructure and thermoelectric properties, Acta Mater. 61 (2013) 3314–3323.

[30] L. Schmidt-Mende, J.L. MacManus-Driscoll, ZnO - nanostructures, defects, and devices, Mater. Today. 10 (2007) 40–48. https://doi.org/10.1016/S1369-7021(07)70078-0.

[31] S.A. Degterov, A.D. Pelton, E. Jak, P.C. Hayes, Experimental study of phase equilibria and thermodynamic optimization of the Fe-Zn-O system, Metall. Mater. Trans. B. 32 (2001) 643–657.

[32] D. Gautam, M. Engenhorst, C. Schilling, G. Schierning, R. Schmechel, M. Winterer, Thermoelectric

properties of pulsed current sintered nanocrystalline Al-doped ZnO by chemical vapour synthesis, J. Mater. Chem. A. 3 (2015) 189–197. https://doi.org/10.1039/C4TA04355C.

[33] C. Chen, B.R. Müller, O.I. Lebedev, F. Giovannelli, G. Bruno, F. Delorme, Effects of impurities on the stability of the low thermal conductivity in Fe 2 TiO 5 ceramics, Mater. Charact. 149 (2019) 111–117. https://doi.org/10.1016/j.matchar.2019.01.021.

[34] G.J. Snyder, E.S. Toberer, Complex thermoelectric materials, Nat. Mater. 7 (2008) 105–114. https://doi.org/10.1038/nmat2090.

Figures

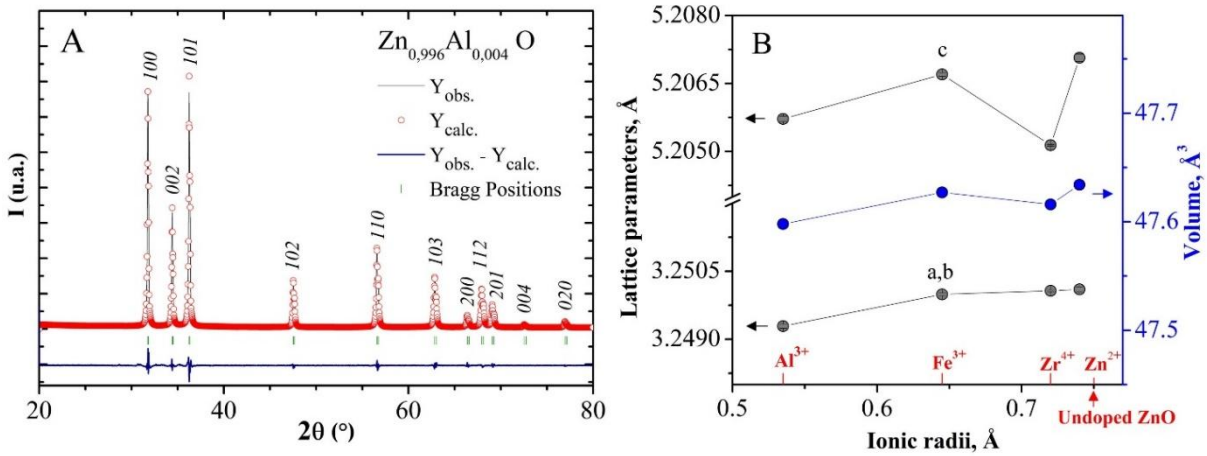

Fig. 1. XRD pattern of as-prepared $Zn_{0.996}Al_{0.004}O$ sample (A) and composition dependence of the lattice parameters and unit cell volume described in terms of the ionic radii [25].

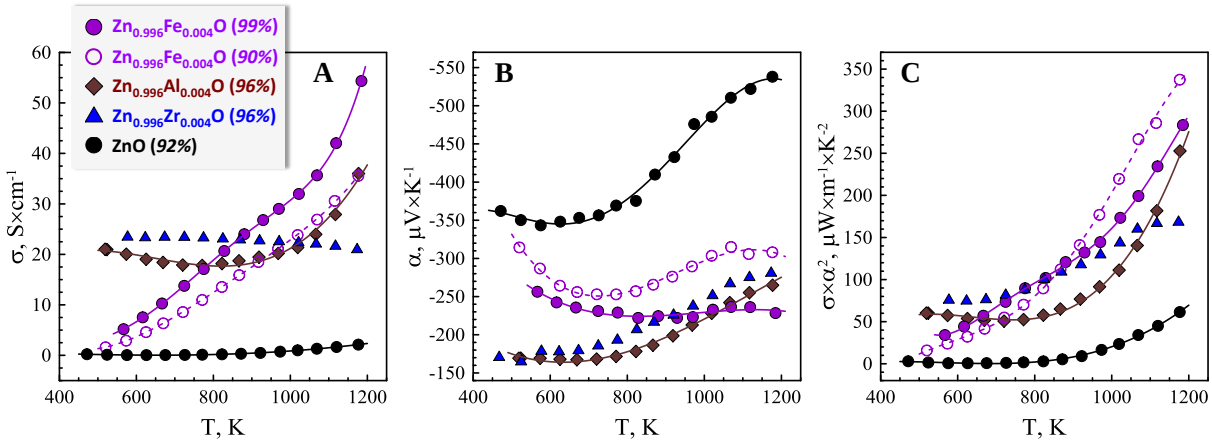

Fig. 2. Temperature dependence of the electrical conductivity (A), Seebeck coefficient (B) and power factor (C), measured in the conditions of relatively fast thermal equilibration of the sample at each temperature.

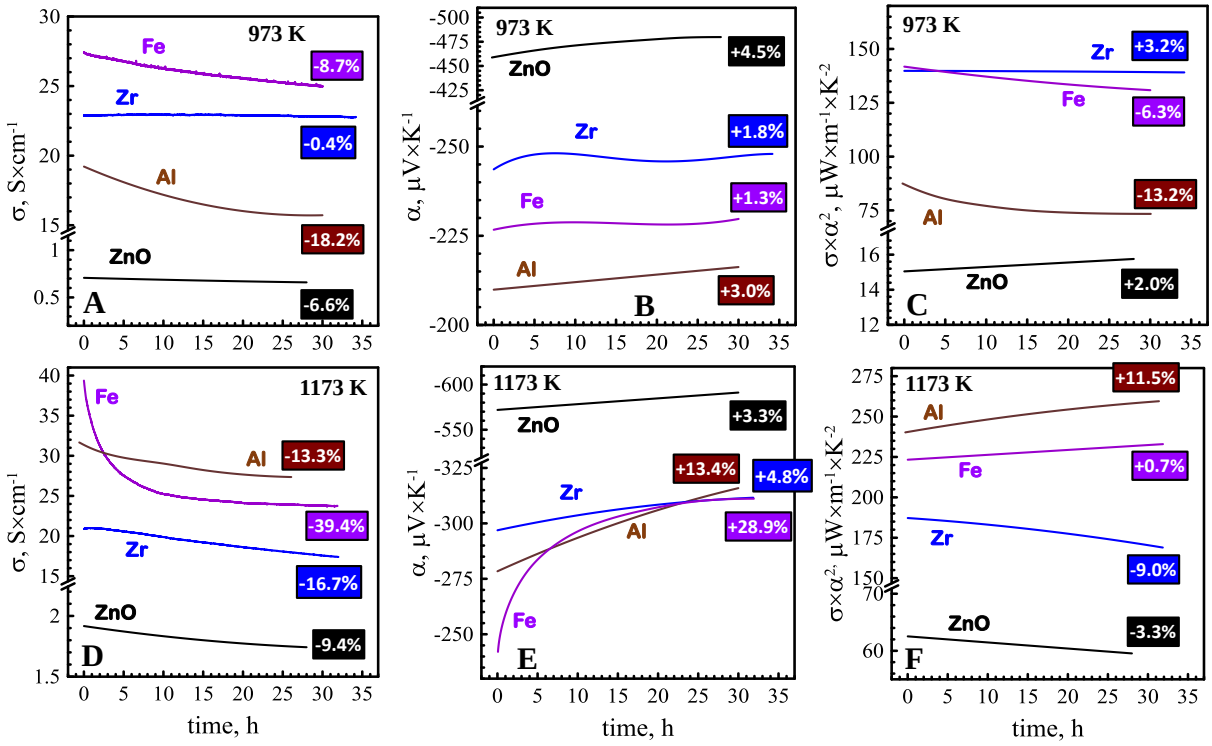

Fig. 3. Time dependence of the electrical conductivity (A, D), Seebeck coefficient (B, E) and power factor (C, F) at 973 K (A–C) and 1173 K (D-F). The extent of evolution for each property is shown in % for each composition.

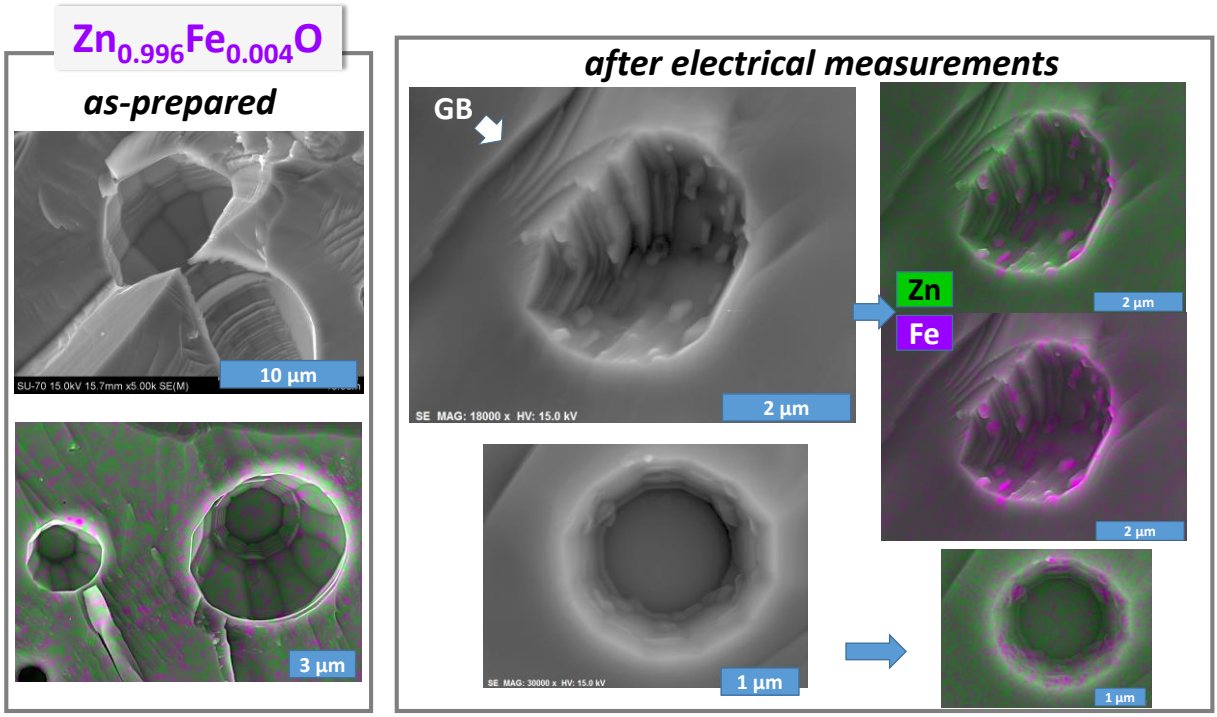

Fig. 4. SEM images and EDS chemical mapping results for the fractured $Zn_{0.996}Fe_{0.004}O$ samples, as-prepared and after electrical characterization.

Figure Captions

Fig. 1. XRD pattern of as-prepared $Zn_{0.996}Al_{0.004}O$ sample (A) and composition dependence of the lattice parameters and unit cell volume described in terms of the ionic radii [20].

Fig. 2. Temperature dependence of the electrical conductivity (A), Seebeck coefficient (B) and power factor (C), measured in the conditions of relatively fast thermal equilibration of the sample at each temperature.

Fig. 3. Time dependence of the electrical conductivity (A, D), Seebeck coefficient (B, E) and power factor (C, F) at 973 K (A–C) and 1173 K (D-F). The extent of evolution for each property is shown in % for each composition.

Fig. 4. SEM images and EDS chemical mapping results for the fractured $Zn_{0.996}Fe_{0.004}O$ samples, as-prepared and after electrical characterization.

Supplementary Information

Click here to download Supplementary Information: Supporting Information.docx

***Declaration of Interest Statement**

Declaration of interests

☒ The authors declare that they have no known competing financial interests or personal relationships that could have appeared to influence the work reported in this paper.

☐The authors declare the following financial interests/personal relationships which may be considered as potential competing interests:

Blanca I. Arias-Serrano – none
Sergey M. Mikhalev – none
Marta C. Ferro – none
David M. Tobaldi – none
Prof. J.R. Frade – none
Dr. A.V. Kovalevsky – none

On behalf of all authors,

Dr. Blanca I. Arias-Serrano,
Postdoctoral Researcher

Department of Materials and Ceramic Engineering, CICECO
University of Aveiro
3810-193 Aveiro
Portugal